



Numerical studies of residual states and scaling effects in laser-directed energy deposition additive manufacturing

Z. Zhang¹ · P. Ge¹ · X. X. Yao¹ · T. Li² · W. W. Liu²

Received: 28 May 2019 / Accepted: 3 April 2020 / Published online: 19 April 2020
© Springer-Verlag London Ltd., part of Springer Nature 2020

Abstract

Sequentially coupled thermo-mechanical model was used to simulate the residual stresses and residual distortions in the directed energy deposition additive manufacturing by laser. The proposed models were validated by comparison with experimental data. Different sizes of components were used to study the scaling effects. Results indicate that the residual stress can be controlled by the component sizes. This phenomenon can be explained by the bending deformation and the temperature fluctuations, especially the cooling rate, in the directed energy deposition additive manufacturing process. Both the bending deformation and the temperature fluctuations can be controlled by the ambient temperature and the designed process parameters. Analytical model was established to show how the components' sizes affect the final residual states in combination with different design parameters.

Keywords Additive manufacturing · Residual stress · Residual distortion · Scaling effect

1 Introduction

Additive manufacturing (AM), as an advanced technology, has gained more attention in recent years [1]. Due to the convenient combination with computer, the components with complex geometries, which are difficult to be achieved using traditional manufacturing technology [2, 3], can be manufactured layer by layer. According to different uses of materials and feeding types, additive manufacturing can be divided into different categories, selected laser sintering [4], selected laser melting [5], and laser-directed energy deposition [3]. The heating energy can be supplied by laser, electron beam [6], arc [7], friction stir [8], cold spray [9], etc.

Due to relatively higher material utilization, directed energy deposition additive manufacturing (DED AM) shows advantages on manufacturing of complex structures with

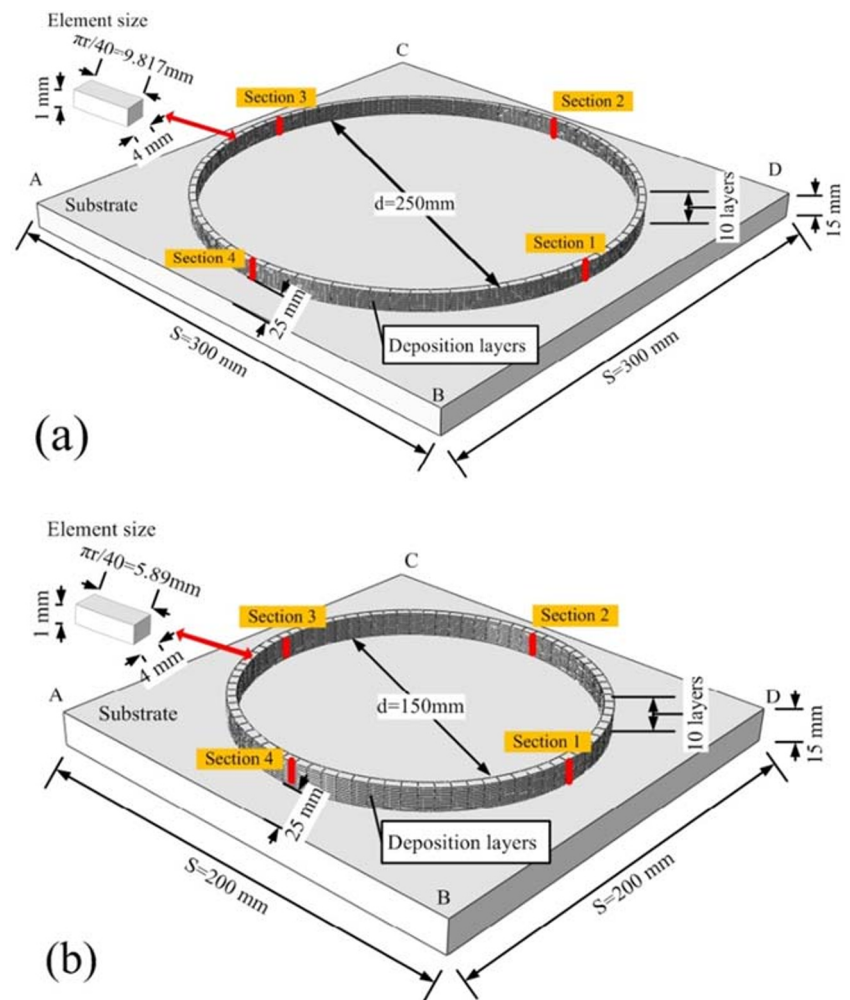
computer design. Temperatures [10–12], residual states [13–16], microstructures [17–19], and mechanical properties [20–22] are key factors for AM, which are studied for controlling and improvement on final product quality. The controlling of residual stresses can be beneficial to controlling of possible defects and cracks in AM. The controlling of residual distortions can be beneficial to improvement of precision of surface in AM. The internal relations between design parameters and controlling of residual stresses and distortions rely on the massive data for investigation, which can be relatively easier to be obtained from theoretical and numerical models. Prediction for controlling of residual stresses and distortions becomes one of the crucial aspects to obtain the manufactured product with higher quality [23]. Lu et al. [13] studied the effect of process parameters on residual stress and distortion. Mukherjee et al. [14] simulated the manufacturing process of dissimilar joints in directed energy deposition additive manufacturing. Biegler et al. [16] calculated the residual deformation of curved additive manufactured component. Cao et al. [24] used 3D transient fully coupled thermomechanical model to calculate the residual stresses and distortions in manufactured component with different parameters. Ali et al. [25] used cylindrical heat source model to study the effect of manufacturing temperature on residual stresses in AM. Vasinonta et al. [26] used thermomechanical models to study the effect of manufacturing parameters on the

✉ Z. Zhang
zhangz@dlut.edu.cn

¹ Department of Engineering Mechanics, Faculty of Vehicle Engineering and Mechanics, State Key Laboratory of Structural Analysis for Industrial Equipment, Dalian University of Technology, Dalian 116024, China

² School of Mechanical Engineering, Dalian University of Technology, Dalian 116024, China

Fig. 1 Geometric models of circle components in DED AM: **a** $r = 125$ mm and **b** $r = 75$ mm



temperature distributions in deposited thin-wall part. An et al. [27] measured residual stress in a curved thin-wall structure made by laser powder bed fusion additive manufacturing processes by neutron diffraction. Somashekara et al. [28] studied the effect of weld-deposition pattern on residual stress in AM.

Although residual states of AM products have been investigated by both numerical models and experiments [13–16, 24–31], the scaling effects on AM product residual states remain unknown. When smaller products are scaled to bigger ones, the strategy on controlling of residual states can become different, which leads to the

needs for development of analytical model to reveal the mechanism on scaling effects. This is the motivation of current work. Sequentially coupled thermomechanical model is utilized to simulate the residual stresses and

Table 1 Modeling parameters in DED AM

Modeling parameters	Value
Laser power (Q_b (W))	1500
Laser beam diameter (d_b (mm))	4
Laser scanning speed (v_b , circular (mm/s))	52.36
Layer height (h (mm))	1
Energy efficiency (η)	0.9

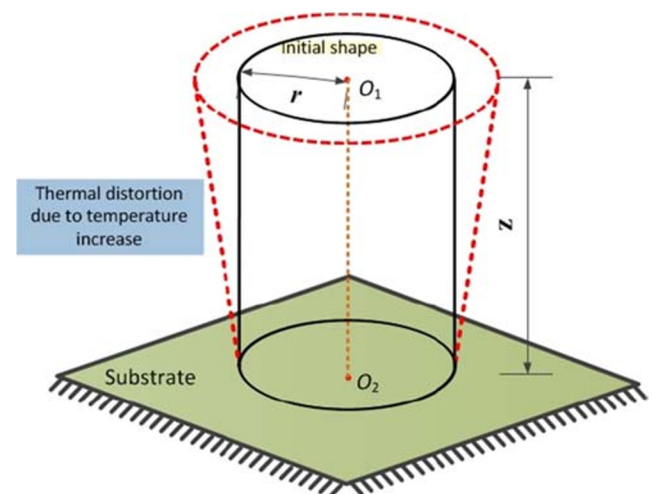
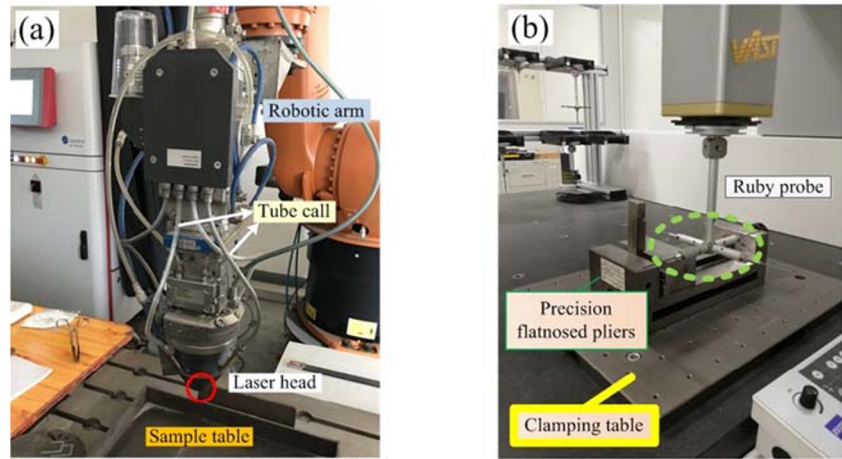


Fig. 2 Analytical model for thermal distortion in cylindrical component

Fig. 3 Experimental equipment in DED AM: **a** laser deposition additive manufacturing system and **b** coordinates measuring machine



distortions in different scales. Experiments are performed for validations. Then, analytical model is established for explanations of scaling effects.

2 Model descriptions

2.1 Finite element model

To simulate the residual states of AM components, a sequential coupled thermal-mechanical finite element model (FEM) is established. The substrate for AM is in dimension of $300 \times 300 \times 15$ mm. Circle components with diameters of 250 and 150 mm are selected to study the scaling effects in AM. The geometries of numerical models of substrate and AM component are shown in Fig. 1. Eighty birth and death elements are used in each layer to model the deposition process of powder particles. At the beginning of DED AM, the build geometries are deactivated (death element). The deactivated elements do not contribute to the thermal and mechanical formulations. With the moving of the laser beam, the build geometries are gradually activated (birth element) element by element and layer by layer.

The temperature dependent physical properties of Ti–6Al–4V are given [24]. In the melt pool of laser metal deposition additive manufacturing, the temperature is always higher than

the melt temperature. This can be found from our experimental observation and also shown in ref. [1]. When the temperature is higher than the melt point, the mechanical properties need to be considered to be very small for the success of the modeling. From the experimental and numerical comparisons, it can be seen that the selection of material properties is appropriate for in prediction of residual states in laser metal deposition AM where melting occurs. And when temperature of Ti–6Al–4V is increased to melt temperature, 1650 °C, the change of thermal conductivity can be found. The change can be modeled by latent heat. In the numerical model, latent heat of 365 kJ/kg is applied when solidus temperature is 1600 °C and liquid temperature is 1660 °C based on ref. [24]. Thus, the values of the material properties in the full temperature range, including the solid and liquid material, are obtained by the linear interpolation according to ref. [13].

2.2 Thermal model

In the modeling of temperature field in DED AM, the governing energy balance can be written as [32]:

$$\rho C \frac{\partial T}{\partial t} = \nabla \cdot (k \nabla T) + q(x, y, z, t) \tag{1}$$

where T is temperature, t is time, k is thermal conductivity coefficient, ρ is density of material, C is specific heat of material, and $q(x, y, z, t)$ is volumetric heat flux. The physical parameters can be considered to be functions of temperature, as revealed in ref. [24]. The cylindrical heat source model is used in the heat transfer model based on the surface heat flux [33], which is written as:

$$q(x, y, z, t) = \frac{3\eta Q_b}{\pi r_b^2 t} \exp \left\{ -3 \frac{(x-x_0)^2 + (y-y_0)^2}{r_b^2} \right\} \tag{2}$$

where $q(x, y, z, t)$ is heat flux, Q_b is laser power, r_b is radius of laser beam, t is layer thickness, η is energy efficiency, and $(x_0,$

Table 2 Parameters in directed energy deposition additive manufacturing

Manufacturing parameters	Value
Powder flow rate (M_p (g/min))	9.15
Powder velocity (v_p (m/s))	1
Laser beam diameter (d_b (mm))	3
Laser scanning speed ($v_{b, \text{plate}}$ (mm/s))	5
Elevating capacity (h_1 (mm))	0.3

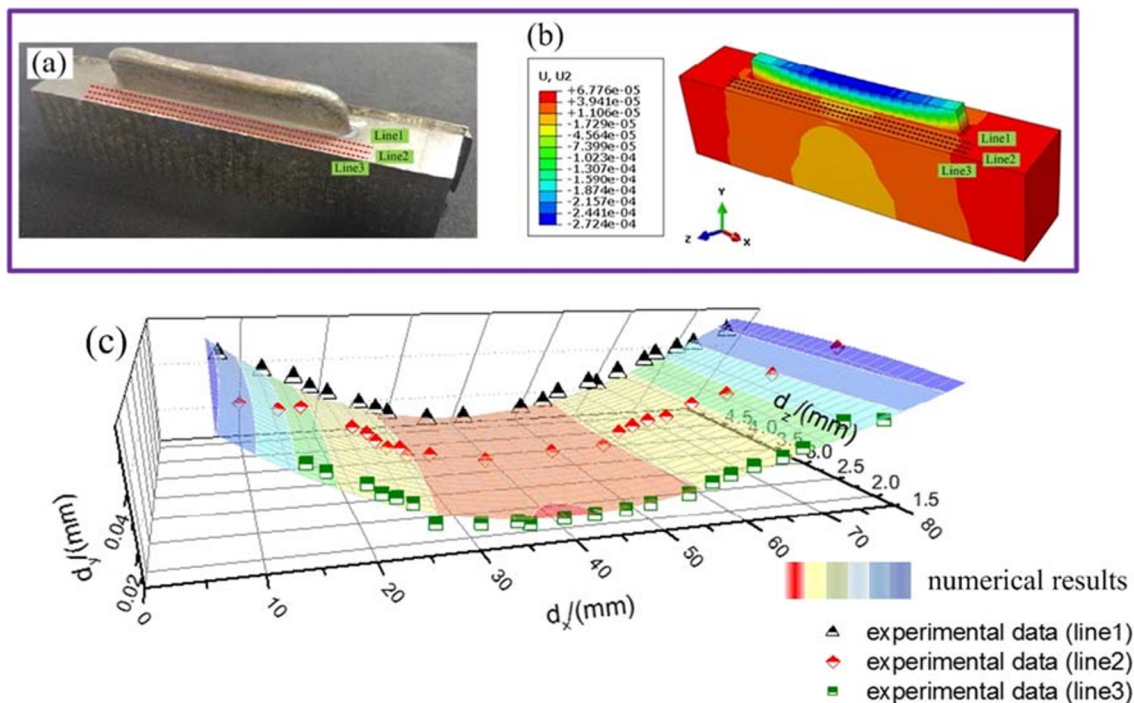


Fig. 4 Comparison between experiment data and numerical results: **a** deposition specimen, **b** residual distortion in FEM, and **c** comparison of residual distortions

y_0) is initial manufacturing point. Thermal convection and radiation boundary conditions are applied to all the free surface, which are written as Eqs. (3) and (4) [34], respectively:

$$q_{\text{conv}} = -h(T - T_a) \quad (3)$$

$$q_{\text{rad}} = -\varepsilon_{\text{rad}} \sigma_{\text{rad}} (T^4 - T_a^4) \quad (4)$$

where $h = 30 \text{ W}/(\text{m}^2/\text{K})$ is convective heat transfer coefficient, $T_a = 20 \text{ }^\circ\text{C}$ is ambient temperature, $\varepsilon_{\text{rad}} = 0.1$ is emissivity of deposition layer, and σ_{rad} is Stefan-Boltzmann constant for radiation. The thermal model is built with the subroutine DFLUX in ABAQUS to model the moving heating on the deposition layer; 56,712 eight-node linear heat transfer elements (DC3D8) are used in the modeling of thermal process in DED AM.

2.3 Mechanical model

After the heat transfer simulation, the temperature history can be further applied in mechanical analysis. The total strain increment ($d\varepsilon$) can be divided into elastic strain increment ($d\varepsilon_e$), plastic strain increment ($d\varepsilon_p$), and thermal strain increment ($d\varepsilon_T$), which can be written as [35]:

$$d\varepsilon = d\varepsilon_e + d\varepsilon_p + d\varepsilon_T \quad (5)$$

where $d\varepsilon_T$ can be written as Eq. (6) with thermal expansion (α).

$$d\varepsilon_T = \alpha dT \quad (6)$$

Based on Hooke's law, the thermal stress increment ($d\sigma$) can be written as:

$$d\sigma = D_e d\varepsilon_e = D_e (d\varepsilon - d\varepsilon_p - d\varepsilon_T) \quad (7)$$

where D_e is material elastic stiffness matrix.

Due to the balance of plastic strain energy when $d\varepsilon_p$ is small, the field function ($F(\sigma, T)$) should satisfy the following equation,

$$\left(\frac{dF}{d\sigma}\right)^T \{d\sigma\} + \frac{\partial F}{\partial T} dT = 0 \quad (8)$$

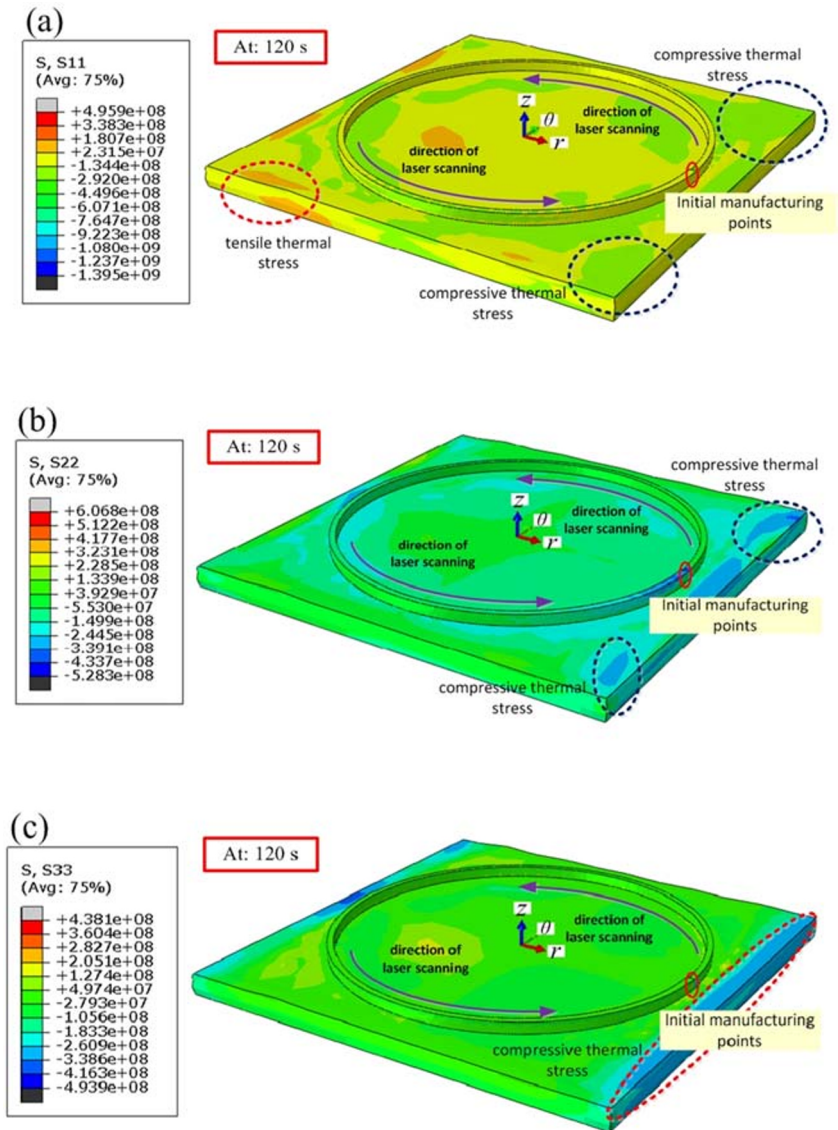
Substituting Eq. (7) into Eq. (8), the following equation can be obtained,

$$\left(\frac{dF}{d\sigma}\right)^T D_e (d\varepsilon - d\varepsilon_p - d\varepsilon_T) + \frac{\partial F}{\partial T} dT = 0 \quad (9)$$

With the solution of Eq. (9) in time domain with backward difference method, thermal stress (σ) can be calculated. In ABAQUS, the temperature history of manufactured product is treated as loads in the mechanical model; 56,712 eight-node linear elements (C3D8R) are used in the mechanical model in DED AM. The full constraints on the bottom surface of substrate are used before the AM product is cooled to ambient temperature. When the AM product is cooled down to ambient temperature, only the rigid body displacements of circular component are constrained.

The manufacturing parameters used in the simulation are listed in Table 1.

Fig. 5 Thermal stresses in circular additive manufacturing product: **a** radial thermal stress, **b** circumferential thermal stress, and **c** vertical thermal stress



2.4 Analytical model

To study the scaling effect on thermal stress and distortion in heating process of circular additive manufactured product,

mechanical analytical model based on thermo-elastic theory is proposed in the current work. The mechanical analytical model of thermal distortion in the heating process in cylindrical component with fix-end constraint is shown in Fig. 2.

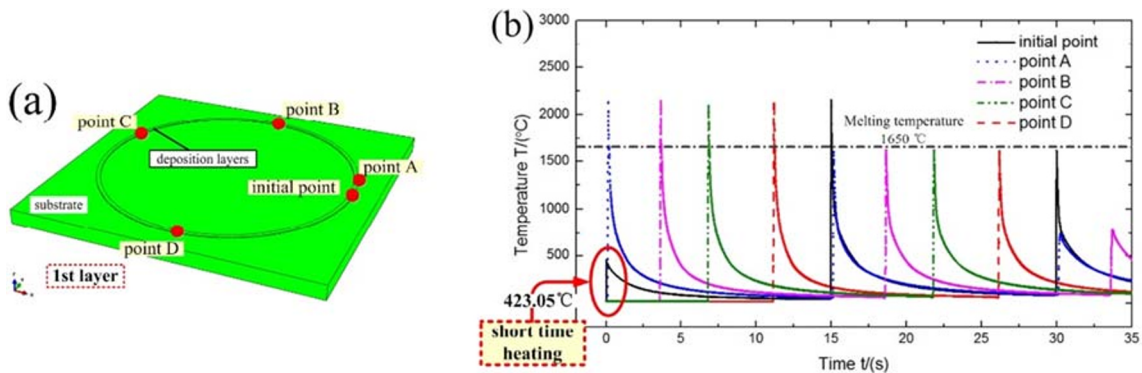


Fig. 6 Comparison of temperature histories at different points in the 1st layer: **a** locations of points and **b** temperature history curves

Fig. 7 Residual distortions of circular additive manufacturing product: **a** distortion of deposition layers and **b** distortion of substrate

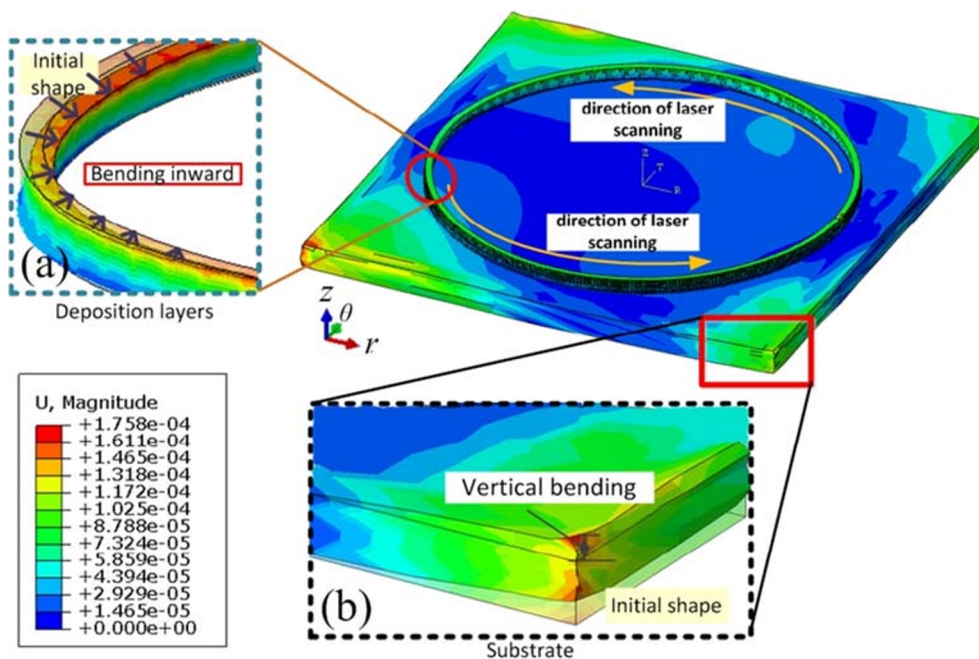
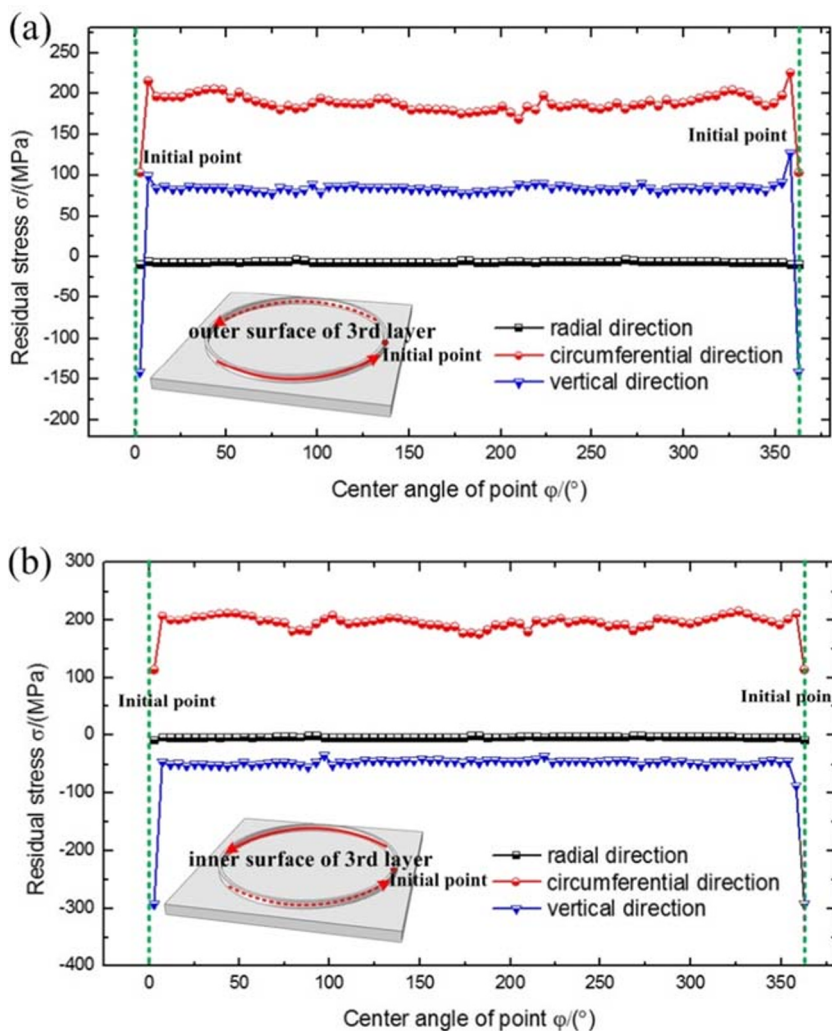


Fig. 8 Residual stresses in 3rd deposition layer in circular additive manufacturing product: **a** on outer surface and **b** on inner surface



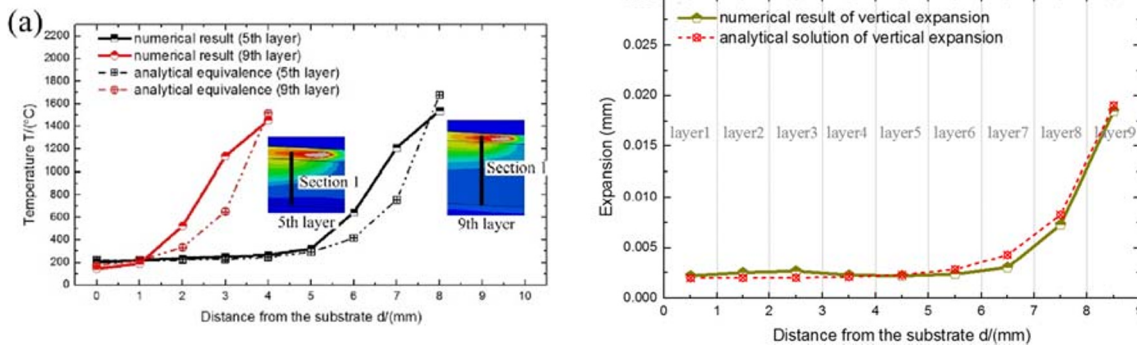


Fig. 9 Distribution of temperature and thermal expansion simulated by numerical model: **a** temperature distributions and **b** radial and vertical expansions in the heating process

Classical basic equations of elasticity mechanics, including equilibrium equations, geometric equations, and physical equations, are used to describe the relationship between thermal expansion (u_{ij}), thermal stress (σ_{ij}), and thermal strain (ε_{ij}) [36]. It is noted that the displacement solution (expansion) (u_{ij}) needs to be 0 when z is 0 due to the fix-end constraint.

In the analysis, the classical equations of elasticity can be simplified with the cylindrical coordinate transformation, $x = r \cdot \cos\theta$, $y = r \cdot \sin\theta$, and $z = z$, and the assumption of axisymmetric temperature distribution in circumferential direction. The simplified equilibrium equations are written as:

$$\frac{\partial \sigma_r}{\partial r} + \frac{\partial \tau_{rz}}{\partial z} + \frac{\sigma_r - \sigma_\theta}{r} = 0 \tag{10}$$

$$\frac{\partial \tau_{rz}}{\partial r} + \frac{\partial \sigma_z}{\partial z} + \frac{\tau_{rz}}{r} = 0 \tag{11}$$

where σ_r is radial normal stress, σ_θ is circumferential normal stress, σ_z is vertical normal stress, and τ_{rz} is shear stress. The simplified geometric equations are written as:

$$\varepsilon_r = \frac{\partial u_r}{\partial r} \tag{12}$$

$$\varepsilon_\theta = \frac{u_r}{r} \tag{13}$$

$$\varepsilon_z = \frac{\partial w}{\partial z} \tag{14}$$

$$\gamma_{rz} = \frac{\partial u_r}{\partial z} + \frac{\partial w}{\partial r} \tag{15}$$

where ε_r is radial normal strain, ε_θ is circumferential normal strain, ε_z is vertical normal strain, γ_{rz} is shear strain, u_r is radial expansion, and w is vertical expansion. The simplified physical equations in thermo-elastic theory are written as:

$$\sigma_r = \frac{E(1-\mu)}{(1+\mu)(1-2\mu)} \left(\varepsilon_r + \frac{\mu}{1-\mu} \varepsilon_\theta + \frac{\mu}{1-\mu} \varepsilon_z \right) - \frac{E\alpha T}{1-2\mu} \tag{16}$$

$$\sigma_\theta = \frac{E(1-\mu)}{(1+\mu)(1-2\mu)} \left(\frac{\mu}{1-\mu} \varepsilon_r + \varepsilon_\theta + \frac{\mu}{1-\mu} \varepsilon_z \right) - \frac{E\alpha T}{1-2\mu} \tag{17}$$

$$\sigma_z = \frac{E(1-\mu)}{(1+\mu)(1-2\mu)} \left(\frac{\mu}{1-\mu} \varepsilon_r + \frac{\mu}{1-\mu} \varepsilon_\theta + \varepsilon_z \right) - \frac{E\alpha T}{1-2\mu} \tag{18}$$

$$\tau_{rz} = \frac{E}{2(1+\mu)} \gamma_{rz} \tag{19}$$

where E is Young’s modulus, μ is Poisson’s ratio, and α is Coefficient of thermal expansion. Substituting Eqs. (12)–(15) and (16)–(19) into Eqs. (10) and (11), the equilibrium equations are written as the function of expansion, u_r and w :

$$\frac{1-\mu}{1-2\mu} \left(\frac{\partial^2 u_r}{\partial r^2} + \frac{1}{r} \cdot \frac{\partial u_r}{\partial r} - \frac{u_r}{r^2} \right) + \frac{1}{2} \cdot \frac{1}{1-2\mu} \cdot \frac{\partial^2 w}{\partial r \partial z} + \frac{1}{2} \cdot \frac{\partial^2 u_r}{\partial z^2} = \frac{\alpha(1+\mu)}{1-2\mu} \cdot \frac{\partial T}{\partial r} \tag{20}$$

$$\frac{1}{2(1-2\mu)} \cdot \frac{\partial^2 u_r}{\partial r \partial z} + \frac{1}{2} \cdot \frac{\partial^2 w}{\partial r^2} + \frac{1}{2(1-2\mu)} \cdot \frac{1}{r} \cdot \frac{\partial u_r}{\partial z} + \frac{1-\mu}{1-2\mu} \cdot \frac{\partial^2 w}{\partial z^2} + \frac{1}{2r} \cdot \frac{\partial w}{\partial r} = \frac{\alpha(1+\mu)}{1-2\mu} \cdot \frac{\partial T}{\partial z} \tag{21}$$

Based on the analytical solutions of expansion in circular additive manufactured product, which are solved by Eqs. (20) and (21), the scaling effect, including radius (r) and height (z) on thermal distortion and stress in heating process in DED AM of circle component can be understood.

3 Experiment

The sample with a dimension of $50 \times 3 \times 6$ mm are built by Ti-6Al-4V powder particles using directed energy deposition additive manufacturing system, which is shown in Fig. 3a. The directed energy deposition additive manufacturing system

Table 3 Coefficients used in analytical model

Coefficient	9th layer
A_{heating}	1.9×10^{-5}
B_{heating}	7.6×10^{-5}
C_{heating}	-1.8×10^{-5}
D_{heating}	220

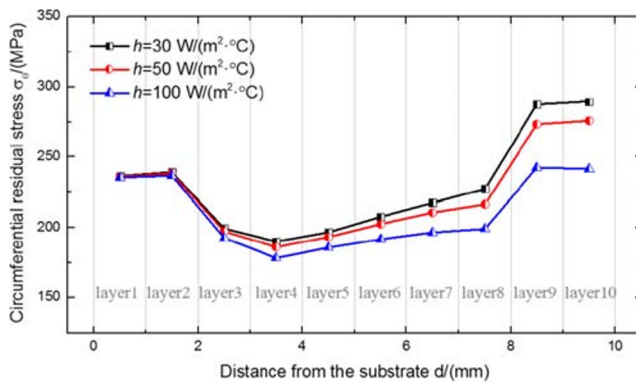


Fig. 10 Effect of cooling rate on circumferential residual stress

comprises ZH 30/60III six-axis manipulator made by Kuka in Germany, LDF 4000-100 Laser Generator made by Laserline in Germany, and YC52 Laser head made by Precitec in Germany.

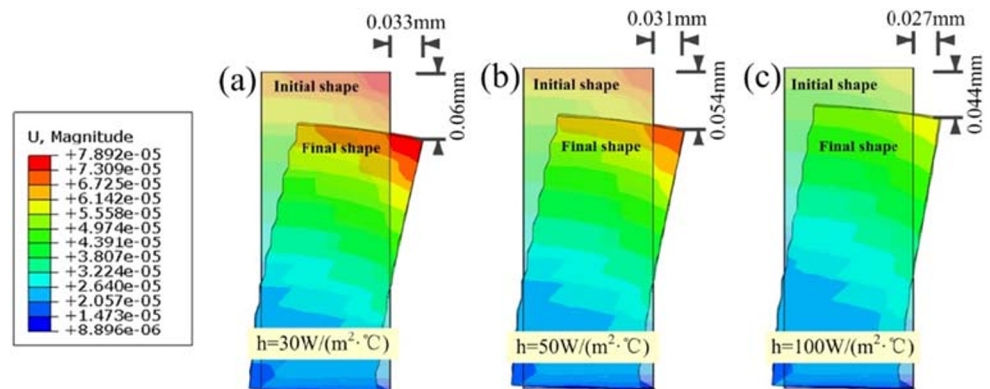
The dimension of substrate is $80 \times 15 \times 20$ mm. The manufacturing parameters used in experiment are listed in Table 2. The laser beam diameter is 3 mm in the experiment. So, in the numerical model in the validation, laser beam diameter is also selected to be 3 mm for comparison. After the manufacturing, residual distortions of the sample are measured by coordinates measuring machine (CMM), as shown in Fig. 3b. The software for data processing is Calypso.

4 Results and discussions

4.1 Comparison between numerical results and experimental data

To validate the correction of coupled thermal-mechanical model in DED AM, numerical model with the same manufacturing parameters is rebuilt to model the residual distortions in experiment. The deposited product is shown in Fig. 4a. The vertical residual distortion distribution in the rebuilt model for simulation is shown in Fig. 4b. The maximum vertical residual distortion along positive direction of y -axis in

Fig. 11 Residual distortions of deposition layers with different cooling rates: **a** $30 \text{ W}/(\text{m}^2 \cdot ^\circ\text{C})$, **b** $50 \text{ W}/(\text{m}^2 \cdot ^\circ\text{C})$, and **c** $100 \text{ W}/(\text{m}^2 \cdot ^\circ\text{C})$



the substrate is 0.067 mm and the one along negative direction of y -axis on the top surface is 0.27 mm. The experimental data and the numerical results of residual distortions are compared in Fig. 4c. The maximum error between experimental data and numerical results of residual distortion is 0.004 mm. The numerical results agree well with the experimental data. The difference between the experimental specimen and the numerical model is caused by the melting and the material flow in the melt pool. This difference only occurs at the end of the specimen. The main part of the specimen and the measured data are not affected by this difference. So, the comparison is still valid to show the success of the proposed model.

4.2 Residual stress and distortion in circle component in DED AM

Using the validated sequentially coupled thermal-mechanical model, thermal stresses, residual stresses, and distortions of circle components in DED AM are calculated. The thermal stresses in additive-manufactured product with the radius of 125 mm at 120 s are shown in Fig. 5. The maximum radial thermal stress, circumferential thermal stress and vertical thermal stress is 495.9, 606.8, and 438.1 MPa, respectively. In DED AM of circular component by laser, the circumferential thermal stress is largest in the stress components. Especially, the asymmetrical distribution of thermal stresses is found in the additive-manufactured circle component. Larger compressive thermal stresses are found in the region near the initial manufacturing point, as shown in Fig. 5. To study the reason for the asymmetrical distribution of thermal stresses, temperature histories at different points, as shown in Fig. 6a, in the 1st layer are shown in Fig. 6b. At the initial point, different temperature histories are found comparing with that of other points. When the manufacturing process begins, the initial point is heated. Due to the fast moving laser to point A, the initial point is not fully heated and a temperature rise of $423.05 \text{ }^\circ\text{C}$ is found. It is different with other points. When the laser beam is moving back to the initial point, it is reheated to $2158 \text{ }^\circ\text{C}$. The expansion formed in the 1st heated

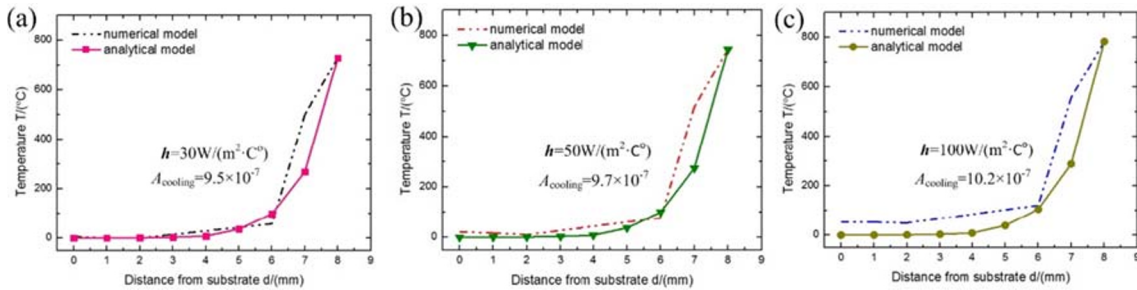


Fig. 12 Comparisons of distributions of decreased temperatures model using FEM and simplified using analytical model with different cooling rates

process leads to the extra compressive thermal stress near the initial point. So, the asymmetrical distribution of thermal stresses in circle component in DED AM is found.

Figure 7 shows the residual distortion in circle component in DED AM. The maximum residual deformation is 0.1758 mm at the corner of substrate. In the deposition layers, bending inward distortion is found, as shown in Fig. 7a. Bending distortion is increased with the increase of build height. The maximum bending inward distortion at the top surface of deposition layers is 0.08 mm. In the substrate, vertical bending distortions are found at the corners. The maximum vertical bending distortion is 0.165 mm, as shown in Fig. 7b. The bending residual distortions greatly influence the geometrical precision of circular additive manufacturing product.

Figure 8 shows the residual stresses in the 3rd deposition layer in circular additive manufacturing product. Different residual stresses are found on the outer surface and inner surface of DED AM circle component. The radial residual stress is very small, comparing with the tensile and vertical residual stress. On the outer surface of the 3rd layer, tensile circumferential and vertical residual stresses are found, except in the special region near the initial point, as shown in Fig. 8a. The maximum tensile circumferential and vertical residual stress is 225.6 and 126.6 MPa, respectively. In the special region, tensile circumferential residual stress is 102.9 MPa and the compressive vertical residual stress is 141.5 MPa. It is caused by the special temperature history at the initial point. On the inner surface, the tensile vertical residual stress is changed to the compressive one, as shown in Fig. 8b. When the residual stress in the special region mentioned above is ignored, the

maximum tensile circumferential residual stress is 211.7 MPa and the maximum compressive vertical residual stress is 80.9 MPa, as shown in Fig. 8b. In the special region near the initial point, tensile circumferential residual stress and compressive vertical residual stress is decreased to 114.3 MPa and increased to 292.6 MPa, respectively. The distribution rules of residual stresses on outer surface and inner surface are similar to the results in ref. [37].

4.3 Analytical solutions of expansion in deposition layer

In Sect. 4.2, the discussion is based on the numerical solutions, which are exactly the same with the experimental observations. But in Sect. 4.3, the analytical model needs to be simplified for feasible solutions. So, the temperature is simplified to be uniform for solutions. According to ref. [38], the temperature distribution in the radial direction can be assumed to be a quadratic function of r . Based on the temperature distributions in different vertical sections in circle component by Xiong [39], temperature distribution in the vertical direction can be assumed to be an exponential function of z . The similar distributed temperatures along the z -axis direction with the existing works [38, 39] are found, as shown in Fig. 9a. The proposed analytical model is only valid for circle shapes due to the use of the cylindrical coordinate system. In the current work, the simplified temperature distribution, which is related with the r , and z , of the circular additive manufactured product, is written as:

$$T_{\text{heating}} = (A_{\text{heating}}r^2 + B_{\text{heating}}) \cdot e^z + C_{\text{heating}} \cdot z + D_{\text{heating}} \quad (22)$$

where A , B , C , and D are coefficients, which relate to temperature distribution. When B_{heating} and C_{heating} satisfy Eqs. (23) and (24), analytical solutions for radial expansion ($u_{r,\text{expansion}}$) and vertical expansion ($w_{\text{expansion}}$) of Eqs. (20) and (21) are solved using the semi-inverse method, which are re-written to be Eqs. (25) and (26), as follows:

$$B_{\text{heating}} = 4A_{\text{heating}} \quad (23)$$

$$C_{\text{heating}} = 2A_{\text{heating}} \cdot \frac{2\mu-1}{1-\mu} \quad (24)$$

Table 4 Coefficients related equivalent temperature distribution with different cooling rates

Cooling rate	30 W/(m ² /°C)	50 W/(m ² /°C)	100 W/(m ² /°C)
A_{heating}	9.5×10^{-7}	9.7×10^{-7}	10.2×10^{-7}
B_{heating}	3.8×10^{-6}	3.88×10^{-6}	4.08×10^{-6}
C_{heating}	-9×10^{-6}	-9.2×10^{-6}	-9.7×10^{-6}
D_{heating}	0	0	0

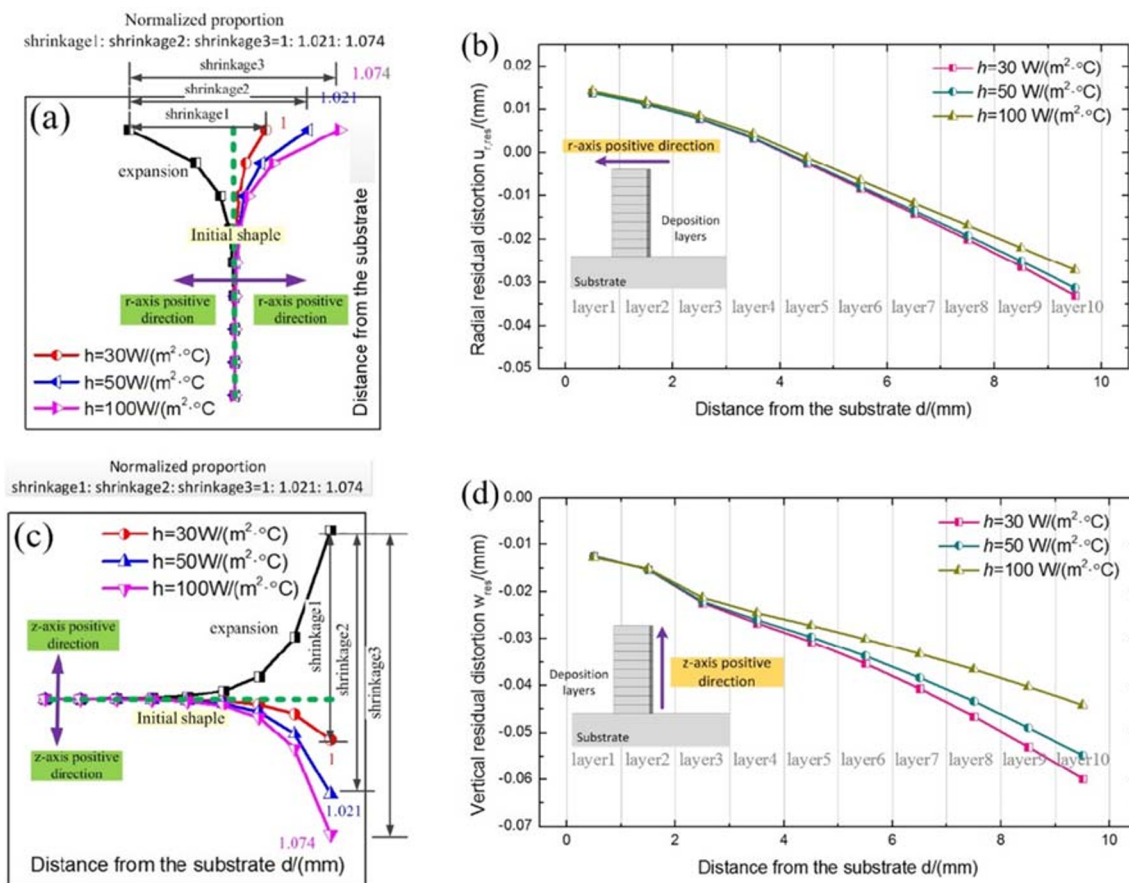


Fig. 13 Effect of cooling rate on residual distortion: **a** normalized radial analytical solutions; **b** radial numerical results; **c** normalized vertical analytical solutions; and **d** vertical numerical results

$$u_{r,expansion} = \frac{2\alpha A_{heating}(1 + \mu)}{(1 - \mu)} \cdot r(e^z - 1) \tag{25}$$

$$w_{expansion} = \frac{\alpha A_{heating}(1 + \mu)}{1 - \mu} \cdot r^2(e^z - 1) \tag{26}$$

The expansion solutions, u_r and w , satisfy the displacement boundary condition in the mechanical analytical model. Substituting Eqs. (25), (26), and (12)–(15) into Eqs.

(16)–(19), the thermal stress in the circular additive manufactured product are calculated, which are written as:

$$\sigma_{r,expansion} = \sigma_{\theta,expansion} = \frac{\alpha EA}{\mu - 1} \cdot r^2 e^z + \frac{2\alpha EA}{\mu - 1} \cdot e^z + \frac{2\alpha EA}{(\mu - 1)(1 - 2\mu)} + \frac{2\alpha EA}{1 - \mu} \cdot z + \frac{D\alpha E}{1 - 2\mu} \tag{27}$$

$$\sigma_{z,expansion} = \frac{4\alpha EA}{\mu - 1} \cdot e^z + \frac{4\mu\alpha EA}{(\mu - 1)(1 - 2\mu)} + \frac{2\alpha EA}{1 - \mu} \cdot z + \frac{D\alpha E}{1 - 2\mu} \tag{28}$$

$$\tau_{rz,expansion} = \frac{2\alpha EA}{1 - \mu} \cdot r e^z - \frac{\alpha EA}{1 - \mu} \cdot r \tag{29}$$

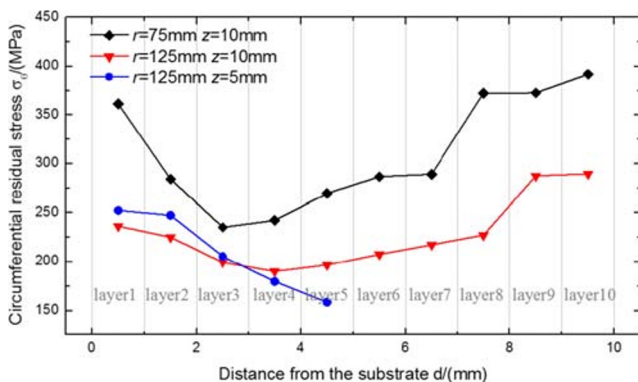


Fig. 14 Scaling effect on circumferential residual stresses in DED AM with different radii and heights of circular component

We take the 9th layer for comparison. When the 9th layer is deposited, the temperature distribution in vertical direction is shown in Fig. 9a. The temperatures need to be changed to an analytical form for uses in the analytical model. The parameters used for this equivalence are summarized in Table 3.

Using the equivalent temperature distribution, the thermal distortion in circular component can be obtained using the analytical model. The comparison of vertical thermal expansion between analytical solutions and numerical results is shown in Fig. 9b. The comparison shows the analytical solutions agree well with the numerical solutions.

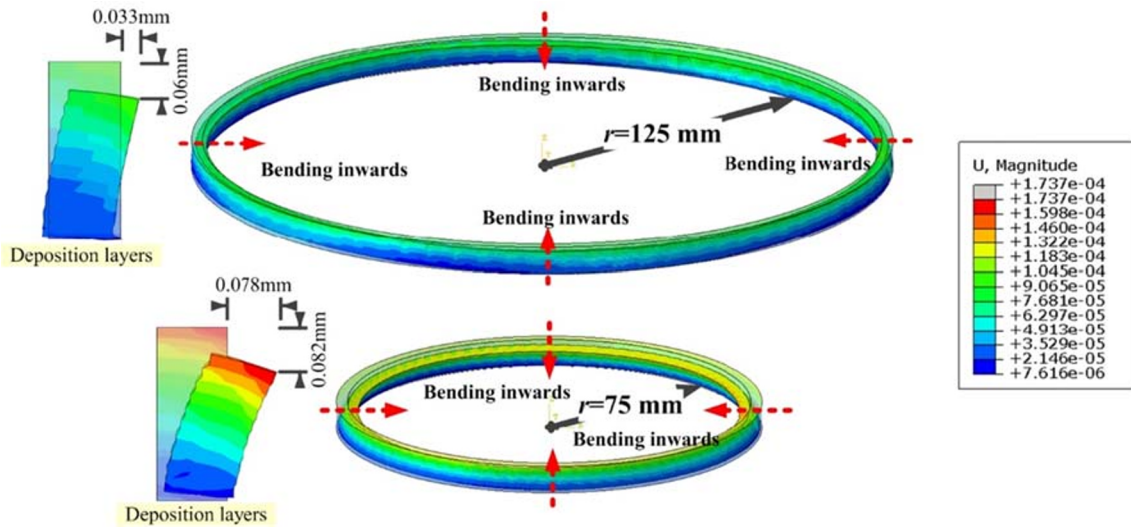
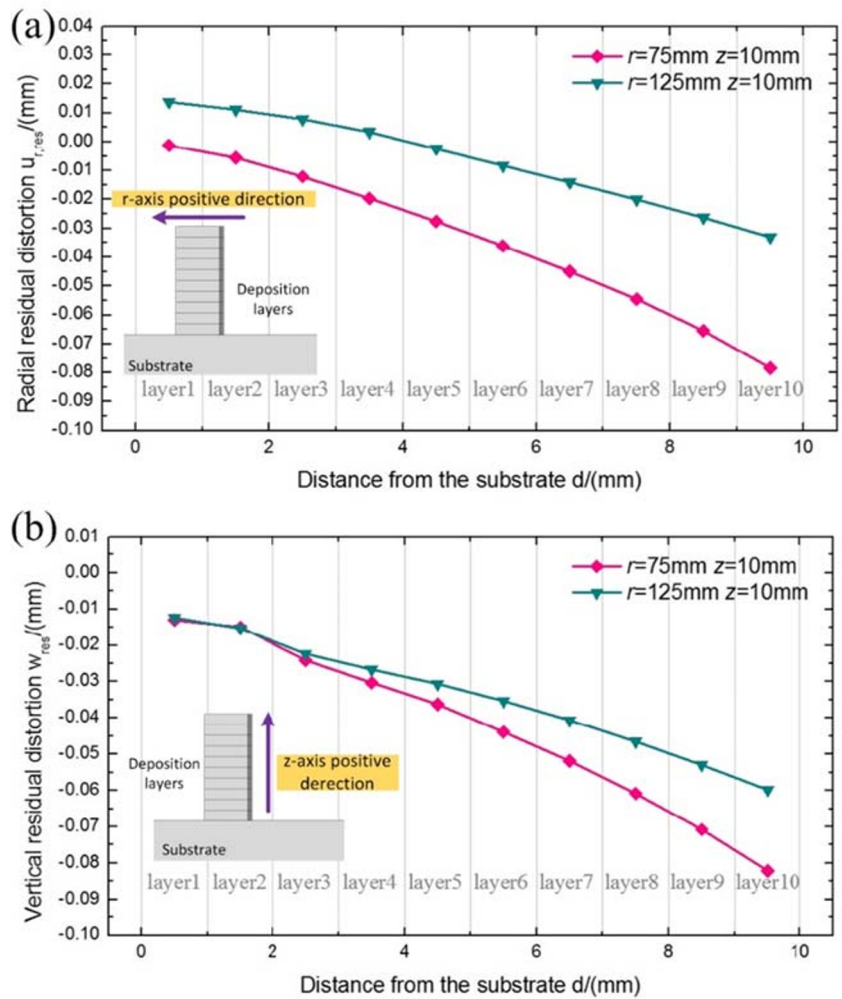


Fig. 15 Residual distortions of deposition layers with different radii

Fig. 16 Effect of radius on residual distortions in DED AM: **a** radial residual distortions and **b** vertical residual distortions



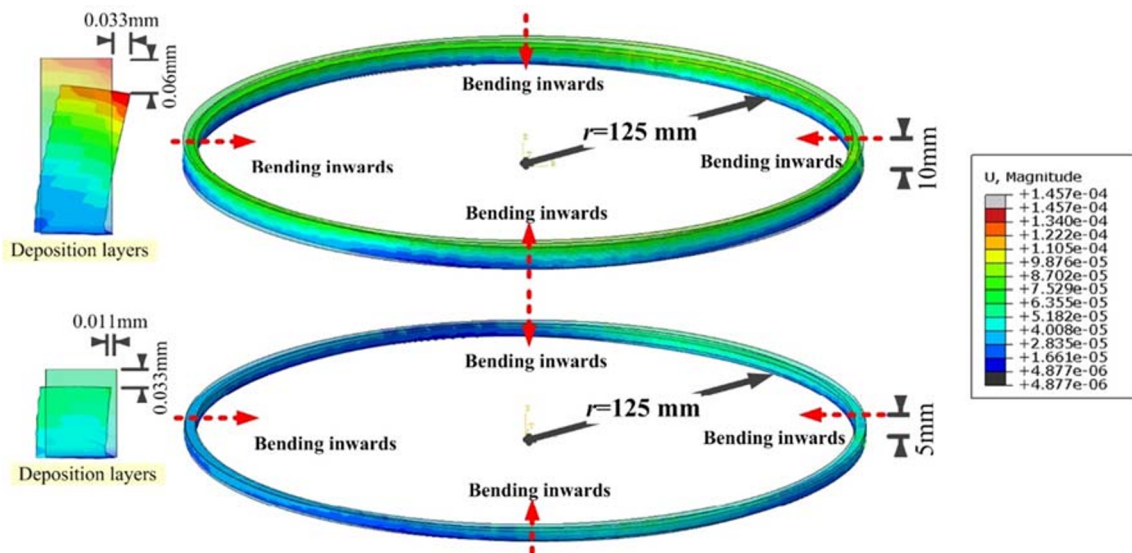
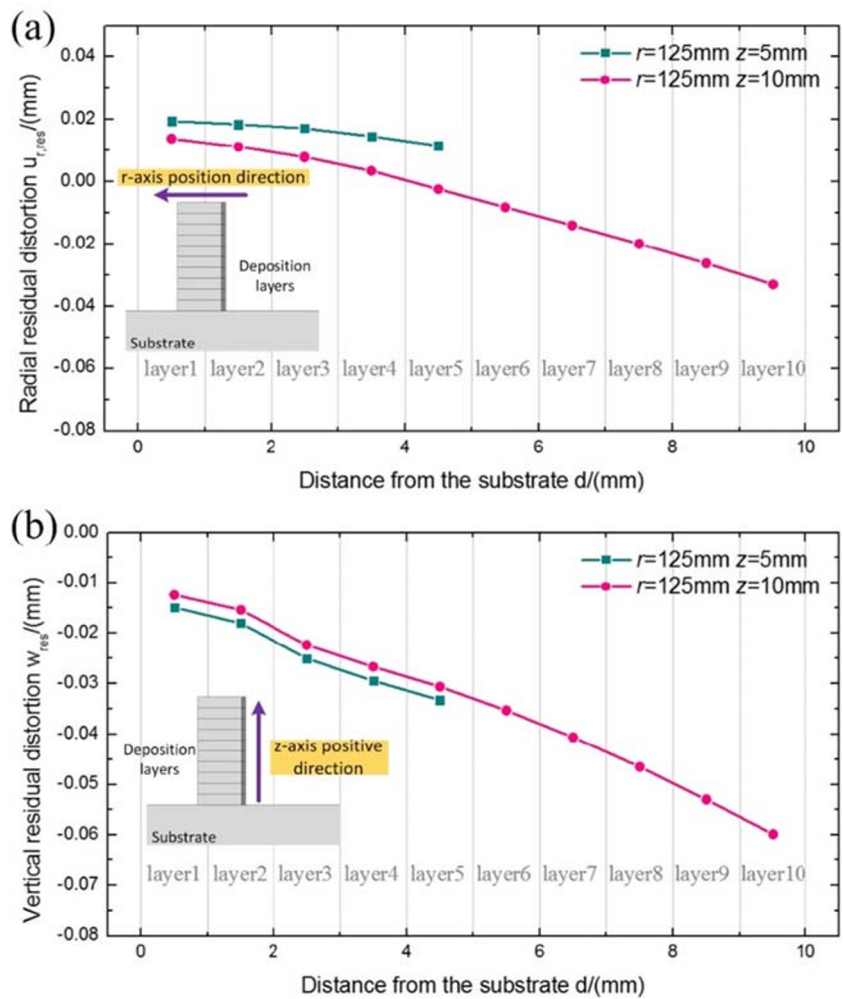


Fig. 17 Residual distortions of deposition layers with different build heights

Fig. 18 Effect of build height on residual distortions in DED AM: **a** radial residual distortions and **b** vertical residual distortions



4.4 Effect of cooling rate on residual stress and distortion

The cooling rate is controlled by the settings of heat connective coefficients. Figure 10 shows the residual stresses with different cooling rates in DED AM. With the increase of cooling rate, decreased circumferential residual stresses are found in the circular additive manufacturing product. The maximum circumferential residual stress is decreased from 289.5 to 241.5 MPa. The distribution of circumferential residual stress in the section of deposition layers is similar with the modeling result of longitudinal residual stress in ref. [13].

As the driving condition of thermal displacement in LMD AM, temperature distribution in deposition layers greatly influences the thermal distortion and the following residual state. In the cooling process, temperature distribution can be also simplified as:

$$T_{cooling} = (A_{cooling}r^2 + B_{cooling}) \cdot e^z + C_{cooling} \cdot z + D_{cooling} \quad (30)$$

where $A_{cooling}$, $B_{cooling}$, $C_{cooling}$, and $D_{cooling}$ are coefficients, which relate to temperature distribution in the cooling process. When $B_{cooling}$ and $C_{cooling}$ satisfy Eqs. (31) and (32), similar shrinkage solutions of $u_{r,shrinkage}$ and $w_{r,shrinkage}$ are written as:

$$B_{cooling} = 4A_{cooling} \quad (31)$$

$$C_{cooling} = 2A_{cooling} \cdot \frac{2\mu-1}{1-\mu} \quad (32)$$

$$u_{r,shrinkage} = \frac{2\alpha A_{cooling}(1+\mu)}{(1-\mu)} \cdot r(e^z-1) \quad (33)$$

$$w_{shrinkage} = \frac{\alpha A_{cooling}(1+\mu)}{1-\mu} \cdot r^2(e^z-1) \quad (34)$$

Figure 11 shows the residual distortion in deposition layers with different cooling rates. When the convective heat transfer coefficient is 30 W/(m²/°C), the radial and vertical residual distortion on the top surface is 0.033 and 0.06 mm, respectively. With the increased convective heat transfer coefficient to 50 W/(m²/°C), the radial and vertical residual distortions are decreased to 0.031 and 0.054 mm. When the convective heat transfer coefficient is increased to 100 W/(m²/°C), the smaller radial residual distortion of 0.027 mm and the smaller vertical residual distortion of 0.044 mm are found on the top surface of deposition layers. The increase of cooling rate in DED AM can greatly decrease the residual distortions of deposition layers.

To study the effect of cooling rate on residual distortions in different deposition layers, distributions of decreased temperatures model using FEM and simplified using analytical model with different cooling rates are shown in Fig. 12. Different coefficients related to the temperature distribution are obtained, as listed in Table 4. With the coefficients, radial and

vertical residual distortions with different cooling rates are shown in Fig. 13. The normalized thermal radial and vertical deformations calculated by analytical solutions are used to explain the different forming processes of residual distortions with different cooling rates, as shown in Fig. 13a, c. In the heating process with the constant of $A_{heating}$, the same expansions calculated by Eqs. (25) and (26) can be found when only the cooling rate is changed. With the increase of cooling rate, $A_{cooling}$ in the temperature distribution is decreased and smaller shrinkages along negative direction of r -axis and negative direction of z -axis calculated by Eqs. (33) and Eqs. (34) are found. When the simulation results are studied, the similar conclusions for the effect of cooling rate on radial and vertical residual distortion can be obtained, as shown in Fig. 13b, d.

4.5 Scaling effect on residual stress and distortion

Figure 14 shows the simulation results of scaling effect on residual stress in DED AM of circle component. With the increase of radius of circle component, the decreased circumferential residual stresses are found in different deposition layers. In the 1st and 10th layers, the tensile circumferential residual stresses are decreased from 361.4 to 236.4 MPa and 391.5 to 289.5 MPa, respectively.

The residual deformations of circle component with the radii of 125 and 75 mm are shown in Fig. 15. The bending inwards deformation of deposition layers is decreased with increase of radius. The maximum radial residual distortion of top surface of deposition layers is decreased from 0.078 to 0.033 mm. And the vertical residual distortion of top surface of deposition layer is decreased from 0.082 to 0.06 mm.

The distributions of residual distortions with different radii are shown in Fig. 16. The decreases of radial and vertical residual distortions are increased with the increase of build height. In the 1st layer, the decreased radial residual distortion is 0.012 mm. In the 5th layer, the decreased radial residual distortion is 0.025 mm. In the 10th layer, the decreased radial residual distortion is increased to 0.045 mm. To analyze the key factor for the changing of residual distortion with different radii, bending model of thin-walled cylinder in mechanics of materials is used in current work. The inertial moment of in-plane bending can be written as [40]:

$$I = \pi r^3 d \quad (35)$$

where d is thickness of deposition layers. With the decrease of r , the inertial moment of deposition layers along negative direction of the r -axis is decreased. Bending stiffness along negative direction of the r -axis is then decreased. So, the bending distortion of deposition layers is increased with the decrease of radius of circle component in DED AM. The inertial moment of in-plane bending is the key factor of bending inwards distortion of deposition layers in circle component.

The residual deformations of circle component with the build heights of 10 and 5 mm are shown in Fig. 17. When the layers with build height of 5 mm are deposited on the substrate, a maximum radial distortion of 0.011 mm along negative direction of the r -axis is found on the top surface of deposition layers. When the build height of layers is increased to 10 mm, the maximum radial distortion along negative direction of the r -axis on the top surface of deposition layers is increased to 0.033 mm. Meanwhile, the vertical residual distortion along negative direction of the z -axis is also increased from 0.033 to 0.06 mm when the build height of layers is increased from 5 to 10 mm. The residual distortions with different build heights are shown in Fig. 18. The distributions of residual distortion in the vertical section are similar because of the same temperature field with the same parameters. The effect of build height of deposition layers can directly be discussed by the result of distribution of vertical residual distortion in the vertical section.

5 Conclusions

Using the validated transient coupled thermal-mechanical FEM, the residual stress and deformation in circle component in DED AM are simulated. The main results are listed as follows:

- (1) Asymmetrical distribution of thermal stress caused by special temperature history at the initial manufacturing point, comparing with thermal stress in other regions of deposition layer.
- (2) With the simplification of temperature in the current work, u_r has a linear relationship with r and an exponential function relationship with z , respectively. Meanwhile, w has a quadratic function relationship with r and an exponential function relationship with z , respectively.
- (3) With the increase of cooling rate, decreased residual stress and distortions can be found in DED AM of circle component.
- (4) The bending distortion of deposition layers is increased with the decrease of radius of circle component in DED AM. The inertial moment of in-plane bending is the key factor of bending inward distortion of deposition layers in circle component.

Conflict of interest The authors declare that they have no conflict of interest.

Funding This study is funded by the National Natural Science Foundation of China (No. 11572074) and Liaoning Provincial Natural Science Foundation (2019-KF-05-07).

References

1. Yang QC, Zhang P, Cheng L, Zhang M, Chyu M, To AC (2016) Finite element modeling and validation of thermomechanical behavior of Ti-6Al-4V in directed energy deposition additive manufacturing. *Addit Manuf* 12:169–177
2. Ghasri-Khouzani M, Peng H, Rogge R, Attardo R, Ostiguy P, Neidig J, Billo R, Hoelale D, Shankar MR (2017) Experimental measurement of residual stress and distortion in additively manufactured stainless steel components with various dimensions. *Mater Sci Eng A* 707:689–700
3. Flores J, Garmendia I, Pujana J (2019) Toolpath generation for the manufacture of metallic components by means of the laser metal deposition technique. *Int J Adv Manuf Technol* 101:2111–2120
4. Fu H, Zhu W, Xu ZF, Chen P, Yan CZ, Zhou K, Shi YS (2019) Effect of silicon addition on the microstructure, mechanical and thermal properties of C-f/SiC composite prepared via selective laser sintering. *J Alloys Compd* 792:1045–1053
5. Lin KJ, Hu KM, Gu DD (2019) Metallic integrated thermal protection structures inspired by the Norway spruce stem: design, numerical simulation and selective laser melting fabrication. *Opt Laser Technol* 115:9–19
6. Yan WT, Ge WJ, Qian Y, Lin S, Zhou B, Liu WK, Lin F, Wagner GJ (2017) Multi-physics modeling of single/multiple-track defect mechanisms in electron beam selective melting. *Acta Mater* 134:324–333
7. Donoghue J, Antonysamy AA, Martina F, Colegrove PA, Williams SW, Prangnell PB (2016) The effectiveness of combining rolling deformation with wire-arc additive manufacture on beta-grain refinement and texture modification in Ti-6Al-4V. *Mater Charact* 114:103–114
8. Zhang Z, Tan ZJ, Li JY, Zu YF, Liu WW, Sha JJ (2019) Experimental and numerical studies of re-stirring and re-heating effects on mechanical properties in friction stir additive manufacturing. *Int J Adv Manuf Technol* 104:767–784. <https://doi.org/10.1007/s00170-019-03917-6>
9. Li WY, Yang K, Yin S, Yang XW, Xu YX, Lupoi R (2018) Solid-state additive manufacturing and repairing by cold spraying: a review. *J Mater Sci Technol* 34:440–457
10. Roberts IA, Wang CJ, Esterlein R, Stanford M, Mynors DJ (2009) A three-dimensional finite element analysis of the temperature field during laser melting of metal powders in additive layer manufacturing. *Int J Mach Tools Manuf* 49:916–923
11. Du J, Wang X, Bai H, Zhao GX, Zhang YB (2017) Numerical analysis of fused-coating metal additive manufacturing. *Int J Therm Sci* 114:342–351
12. Heigel JC, Michaleris P, Reutzel EW (2015) Thermo-mechanical model development and validation of directed energy deposition additive manufacturing of Ti-6Al-4V. *Addit Manuf* 5:9–19
13. Lu XF, Lin X, Chiumenti M, Cervera M, Hu YL, Ji XL, Ma L, Yang HO, Huang WD (2019) Residual stress and distortion of rectangular and S-shaped Ti-6Al-4V parts by directed energy deposition: Modelling and experimental calibration. *Addit Manuf* 26:166–179
14. Mukherjee T, Zuback JS, Zhang W, DebRoy T (2019) Residual stresses and distortion in additively manufactured compositionally graded and dissimilar joints. *Comput Mater Sci* 143:325–337
15. Heigel JC, Phan TQ, Fox JC, Gnaupel-Herold TH (2018) Experimental investigation of residual stress and its impact on machining in hybrid additive/subtractive manufacturing. *Proc Manuf* 26:929–940
16. Biegler M, Marko A, Graf B, Rethmeier M (2018) Finite element analysis of in-situ distortion and bulging for an arbitrarily curved additive manufacturing directed energy deposition geometry. *Addit Manuf* 24:264–272

17. Zinovieva O, Zinoviev A, Ploshikhin V (2018) Three-dimensional modeling of the microstructure evolution during metal additive manufacturing. *Comput Mater Sci* 141:207–220
18. Zhang Z, Tan ZJ, Yao XX, Hu CP, Ge P, Wan ZY, Li JY, Wu Q (2019) Numerical methods for microstructural evolutions in laser additive manufacturing. *Comput Math Appl* 78:2296–2307. <https://doi.org/10.1016/j.camwa.2018.07.011>
19. Su JZ, Xiao MZ, Zhang ZJ, Ye ZP, Jin X, Yang YC (2017) Microstructural morphology and evolution of austenite stainless steel deposited using pulsed laser and wire. *Int J Adv Manuf Technol* 93:3357–3370
20. Ren B, Zhang M, Chen CJ, Wang XN, Zou T, Hu ZR (2017) Effect of heat treatment on microstructure and mechanical properties of stellite 12 fabricated by laser additive manufacturing. *J Mater Eng Perform* 26:5404–5413
21. Ge P, Zhang Z, Tan ZJ, Hu CP, Zhao GZ, Guo X (2019) An integrated modeling of process-structure-property relationship in laser additive manufacturing of duplex titanium alloy. *Int J Therm Sci* 140:329–343
22. Yan WT, Lin S, Kafka OL, Yu C, Liu ZL, Lian YP, Wolff S, Cao J, Wagner GJ, Liu WK (2018) Modeling process-structure-property relationships for additive manufacturing. *Front Mech Eng* 13:482–492
23. Zhang Z, Ge P, Zhao GZ (2017) Numerical studies of post weld heat treatment on residual stresses in welded impeller. *Int J Press Vessel Pip* 153:1–14
24. Cao J, Gharghoury MA, Nash P (2016) Finite-element analysis and experimental validation of thermal residual stress and distortion in electron beam additive manufactured Ti-6Al-4V build plates. *J Mater Process Technol* 237:409–419
25. Ali H, Ghadbeigi H, Mumtaz K (2018) Residual stress development in selective laser-melted Ti6Al4V: a parametric thermal modelling approach. *Int J Adv Manuf Technol* 97:2621–2633
26. Vasinonta A, Beuth JL, Griffith M (2007) Process maps for predicting residual stress and melt pool size in the laser-based fabrication of thin-walled structures. *J Manuf Sci Eng* 129:101–109
27. An K, Yuan L, Dial L, Spinnelli I, Stoica AD, Gao Y (2017) Neutron residual stress measurement and numerical modeling in a curved thin-walled structure by laser powder bed fusion additive manufacturing. *Mater Des* 135:122–132
28. Somashekara MA, Naveenkumar M, Kumar A, Viswanath C, Simhambhatla S (2017) Investigations into effect of weld-deposition pattern on residual stress evolution for metallic additive manufacturing. *Int J Adv Manuf Technol* 90:2009–2025
29. Ghasri-Khouzani M, Peng H, Rogge R, Attardo R, Ostiguy P, Neidig J, Billo R, Hoelzle D, Shankar MR (2017) Experimental measurement of residual stress and distortion in additively manufactured stainless steel components with various dimensions. *Mater Sci Eng A* 707:689–700
30. Kalentics N, Boillat E, Peyre P, Gorny C, Kenel C, Leinenbach C, Jhabvala J, Logé RE (2017) 3D laser shock peening—a new method for the 3D control of residual stresses in selective laser melting. *Mater Des* 130:350–356
31. Fergani O, Berto F, Welo T, Liang SY (2017) Analytical modelling of residual stress in additive manufacturing. *Fatigue Fract Eng Mater Struct* 40:971–978
32. Kundakcioglu E, Lazoglu I, Poyraz Ö, Yasa E, Cizicioğlu N (2018) Thermal and molten pool model in selective laser melting process of Inconel 625. *Int J Adv Manuf Technol* 95:3977–3984
33. Manvatkar VD, Gokhale AA, Reddy GJ, Venkataramana A, De A (2011) Estimation of melt pool dimensions, thermal cycle, and hardness distribution in the laser-engineered net shaping process of austenitic stainless steel. *Metall Mater Trans A* 42:4080–4087
34. Zhang ZD, Huang YZ, Kasinathan AR, Shahabad SI, Ali U, Mahmoodkhani Y, Toyserkani E (2019) 3-Dimensional heat transfer modeling for laser powder-bed fusion additive manufacturing with volumetric heat sources based on varied thermal conductivity and absorptivity. *Opt Laser Technol* 109:297–312
35. Biegler M, Graf B, Rethmeier M (2018) In-situ distortions in LMD additive manufacturing walls can be measured with digital image correlation and predicted using numerical simulations. *Addit Manuf* 20:101–110
36. Wu JL (2011) *Elasticity*. Higher Education Press, Beijing (in Chinese)
37. Li R, Xiong J, Lei YY (2019) Investigation on thermal stress evolution induced by wire and arc additive manufacturing for circular thin-walled parts. *J Manuf Process* 40:59–67
38. Wang HG (1989) *Outline of Thermoelasticity*. Tsinghua University Press, Beijing (in Chinese)
39. Xiong J, Lei YY, Li R (2017) Finite element analysis and experimental validation of thermal behavior for thin-walled parts in GMAW-based additive manufacturing with various substrate preheating temperatures. *Appl Therm Eng* 126:43–52
40. Ji SY (2018) *Mechanics of materials*. Science Press, Beijing (in Chinese)

Publisher's note Springer Nature remains neutral with regard to jurisdictional claims in published maps and institutional affiliations.